Our wide range of CT phantoms along with Catphan® phantoms, now paired with Smári Image Analysis.

Quantitative tests to measure the maximum performance of modern multi-slice and CBCT scanners.

The Phantom Laboratory manufactures high-precision phantoms coupled with Smári image analysis service and innovative custom solutions for the medical imaging and radiation therapy fields.

Click to see our latest phantoms and schedule a demo of our Smári image analysis service.

Fast dose optimization for rotating shield brachytherapy

Myung Cho
Department of Electrical and Computer Engineering, University of Iowa, 4016 Seamans Center, Iowa City, IA 52242, USA

Xiaodong Wu[a)]
Department of Electrical and Computer Engineering, University of Iowa, 4016 Seamans Center, Iowa City, IA 52242, USA
Department of Radiation Oncology, University of Iowa, 200 Hawkins Drive, Iowa City, IA 52242, USA

Hossein Dadkhah
Department of Biomedical Engineering, University of Iowa, 1402 Seamans Center, Iowa City, IA 52242, USA

Jirong Yi
Department of Electrical and Computer Engineering, University of Iowa, 4016 Seamans Center, Iowa City, IA 52242, USA

Ryan T. Flynn and Yusung Kim
Department of Radiation Oncology, University of Iowa, 200 Hawkins Drive, Iowa City, IA 52242, USA

Weiyu Xu
Department of Electrical and Computer Engineering, University of Iowa, 4016 Seamans Center, Iowa City, IA 52242, USA

(Received 17 April 2017; revised 25 June 2017; accepted for publication 17 July 2017; published 11 September 2017)

Purpose: To provide a fast computational method, based on the proximal graph solver (POGS) – A convex optimization solver using the alternating direction method of multipliers (ADMM), for calculating an optimal treatment plan in rotating shield brachytherapy (RSBT). RSBT treatment planning has more degrees of freedom than conventional high-dose-rate brachytherapy due to the addition of emission direction, and this necessitates a fast optimization technique to enable clinical usage.
Methods: The multi-helix RSBT (H-RSBT) delivery technique was investigated for five representative cervical cancer patients. Treatment plans were generated for all patients using the POGS method and the commercially available solver IBM ILOG CPLEX. The rectum, bladder, sigmoid colon, high-risk clinical target volume (HR-CTV), and HR-CTV boundary were the structures included in our optimization, which applied an asymmetric dose-volume optimization with smoothness control. Dose calculation resolution was $1 \times 1 \times 3$ mm^3 for all cases. The H-RSBT applicator had 6 helices, with 33.3 mm of translation along the applicator per helical rotation and 1.7 mm spacing between dwell positions, yielding 17.5° emission angle spacing per 5 mm along the applicator.
Results: For each patient, HR-CTV D_{90}, HR-CTV D_{100}, rectum D_{2cc}, sigmoid D_{2cc}, and bladder D_{2cc} matched within 1% for CPLEX and POGS methods. Also, similar EQD2 values between CPLEX and POGS methods were obtained. POGS was around 18 times faster than CPLEX. For all patients, total optimization times were 32.1–65.4 s for CPLEX and 2.1–3.9 s for POGS.
Conclusions: POGS reduced treatment plan optimization time approximately 18 times for RSBT with similar HR-CTV D_{90}, organ at risk (OAR) D_{2cc} values, and EQD2 values compared to CPLEX, which is significant progress toward clinical translation of RSBT. © *2017 American Association of Physicists in Medicine* [https://doi.org/10.1002/mp.12486]

Key words: brachytherapy, cancer treatment planning, gynecological cancer, optimization, rotating shield brachytherapy

1. INTRODUCTION

High-dose-rate brachytherapy (HDR-BT) involves placing a radiation source inside of or adjacent to a target organ, that is, tumor. Conventional HDR-BT uses an unshielded brachytherapy source with a radially symmetric dose distribution,[1,2] which limits the intensity modulation capacity of the approach. Rotating-shield brachytherapy (RSBT) has a rotating radiation-attenuating shield around a brachytherapy source. The RSBT concepts for single-catheter treatment[3] and multicatheter treatment[4] were introduced by Ebert.

In the multihelix RSBT (H-RSBT) treatment[5] (Fig. 1), a radiation source travels inside a tandem of Henschke Applicator having helical keyways. A keyway is a helical slot wound inside of the applicator, which provides a pathway for the shield to move along, when the coupled source is translated, to ensure its correct orientation. While moving along the applicator for a given keyway, the partial shield rotates around the radiation source simultaneously. Due to the design of the applicator, the position of the source in the applicator dictates the direction of the open part of the shield. In traveling along each keyway, the radiation source stops at designated dwell positions. Intensity-modulated dose distributions can be delivered to the target with reduced dose exposure to nontarget organs by controlling the treatment time in an optimal manner for each dwell position. Hence, a radiation

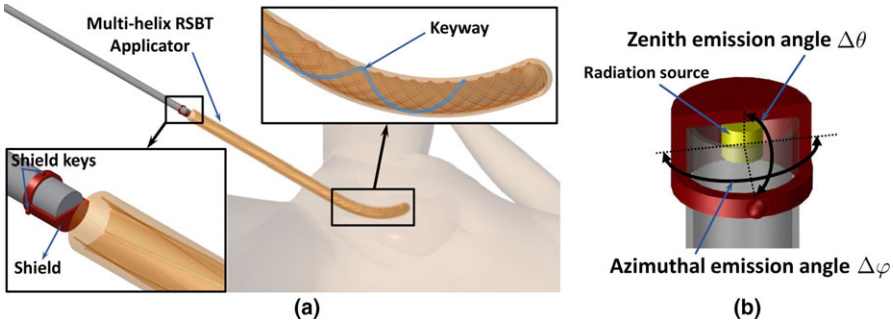

FIG. 1. (a) Illustration of multihelix rotating shield brachytherapy (H-RSBT) system. Adapted from "Multihelix rotating shield brachytherapy for cervical cancer," by H. Dadkhah, Y. Kim, X. Wu, and R. T. Flynn, Medical Physics 42, 6579-6588 (2015). Copyright 2015 by the American Association of Physicists in Medicine. (b) Partially shielded radiation source. [Color figure can be viewed at wileyonlinelibrary.com]

source with rotating shields can deliver more conformal dose distributions than an unshielded radiation source.[5]

Unlike the conventional HDR-BT optimization using inverse planning based on given clinical prescription,[6–12] the RSBT optimization problem has the additional optimization variables of radiation exposure time at each angle of the shield. Due to the increased degrees of freedom in RSBT, RSBT optimization is more difficult than that for the conventional HDR-BT. In addition, it is desirable to quickly obtain optimal treatment plans in RSBT to enable clinical usage. To achieve this, researchers have used the dose-surface optimization (DSO) method,[13,14] which minimizes the total dose errors over only voxels on the HR-CTV surface. Instead of dealing with only voxels on the HR-CTV surface, Liu et al.[15] included voxels on the surface of HR-CTV as well as voxels inside of tumor in certain distance range from the applicator in their optimization problem. Additionally, the authors used the total variation (TV) norm penalty in the optimization problem to make smooth changes in the emission times of adjacent beams in the treatment process to facilitate the efficient delivery of an RSBT plan. This optimization approach for RSBT is called asymmetric dose-volume optimization with smoothness control (ADOS).

In this paper, the ADOS optimization problem, which is a large-scale RSBT optimization problem, is investigated. A fast computational method is proposed to solve the ADOS optimization problem for the optimal cancer treatment planning for RSBT. Liu et al. used a commercial optimization solver called CPLEX.[15,16] In order to efficiently solve the ADOS optimization problem, an optimization method based on the proximal graph solver (POGS),[17] which is a solver using the alternating direction method of multipliers (ADMM), was designed. For this purpose, the closed-form formulas for the proximal operators used in POGS were derived. Furthermore, the proposed method was applied to H-RSBT, which is a mechanically feasible delivery technique for RSBT proposed by Dadkhah et al.[5] In this paper, the proposed methodology was applied to the treatment of cervical cancer, even though the method is also applicable to other types of cancer such as breast cancer and prostate cancer.

2. MATERIALS AND METHODS

2.A. Delivery method

In order to deliver the radiation dose to a target organ, a mechanically feasible delivery technique for RSBT, called H-RSBT,[5] is considered. Figure 1 shows the illustration of the H-RSBT method. The shield opening is represented by the *azimuthal* and *zenith* emission angles, denoted by $\Delta\varphi$ and $\Delta\theta$, respectively.

In H-RSBT, an Xoft Axxent radiation source, inside its cooling catheter, with a freely rotating partial radiation shield is translated inside an applicator with six helical keyways carved out of the inner wall. The six keyways are evenly spaced by 60° on the applicator cross section, and each keyway has a helical pitch of one rotation per 33.3 mm of translation. The partial shield has a protruding key that travels down a given keyway, and, due to the helical design of the keyways, the shield rotates about the radiation source as the source catheter is translated, and the emission angle of the shield is fixed for a given keyway and translational dwell position. As the H-RSBT applicator has six helices, with 33.3 mm of translation along the applicator per helical rotation and 1.7 mm spacing between dwell positions, it yields 17.5° of rotation for the shield per 5 mm (standard dwell position spacing) of its translation along the applicator. The dose calculation resolution was $1 \times 1 \times 3$ mm^3 for all cases. The transmission through the shield was 0.1% and approximated to be 0% for the dose calculation. For all treatment plans, an azimuthal emission angle of 45° was used. The zenith emission angle of the modeled shields was an asymmetric 116°, which is consistent with previous work.[5]

2.B. Radiation source model and dose calculation

For H-RSBT, the delivery is parameterized by keyway number and dwell position number along the keyway. To quantitatively describe the structure of high-dose regions formed by a partially shielded source, the notation of *beamlet* is introduced. A beamlet, denoted by $D_i(j,b)$, is defined as the dose rate at point $\vec{r}_i$ with the shielded source positioned at the j-th dwell position while the shield is aligned with the b-th keyway.

To calculate the beamlet, the TG-43 dose calculation model of Rivard et al.[18] is used. The radiation source is assumed to be partially shielded 50 kVp Xoft Axxent™ (Sunnyvale, CA, USA). To be consistent with previous work,[13,14,19] it is assumed that the dose to the points blocked by the shield is 0, since the transmission rate from 50 kVp Xoft Axxent™ can be controlled to be less than 0.1% when using a 0.5 mm tungsten shield.[13,14] Then, the radiation dose amount at the point $\vec{r}_i$, denoted by d_i, can be quantified as a time-weighted sum of all beamlets as follows:

$$d_i = \sum_{j,b} D_i(j,b) t_{j,b}, \tag{1}$$

where $t_{j,b}$ is the dwell time of beamlet $D_i(j,b)$.

The next subsection describes the RSBT optimization problem having asymmetric penalty parameters for HR-CTV and organs at risk (OARs), with TV regulation term for smoothness in the beamlet emission times.

2.C. Optimization problem for cancer treatment planning in RSBT

2.C.1. Problem formulation

Let $t \in \mathbb{R}^{mn\times 1}$ be the beamlet emission time vector for all keyways and all dwell positions, where m and n are the number of keyways, that is, $m = 6$, and the number of dwell positions along a keyway, respectively. t can be obtained by vectorizing $t_{j,b}$ in Eq. (1); namely, the vector $t \in \mathbb{R}^{mn\times 1}$ is a concatenated vector, which is expressed as $t = [t[1]^T, t[2]^T, \ldots, t[m]^T]^T$, where $t[j] \in \mathbb{R}^{n\times 1}$ is the dwell time vector for all the beamlets along a keyway, and the super-script T represents the transpose. Let us define a concatenated dose rate matrix $D = [D[1], D[2], \ldots, D[m]] \in \mathbb{R}^{l\times mn}$, where $D[j] \in \mathbb{R}^{l\times n}$, $j = 1,\ldots,m$, is the dose rate matrix for the j-th selected keyway, and l is the number of voxels of interest (VOIs). The whole index set for voxels of interest is denoted as $\mathcal{I}_{VOIs}$ and the index set for HR-CTV, bladder, rectum, sigmoid, and normal tissue around the HR-CTV as $\mathcal{I}_{tumor}$, $\mathcal{I}_{bladder}$, $\mathcal{I}_{rectum}$, $\mathcal{I}_{sigmoid}$, and $\mathcal{I}_{normal}$ respectively. The dose rate matrix D has information about dose rate delivered to each tissue point in $\mathcal{I}_{VOIs}$ from each beamlet.

The following RSBT optimization problem is considered, where the objective function includes a term representing the quadratic dosimetric objective function, and a term that regulates the total variation for smooth beamlet emission times. Equation (2) represents an optimization problem that can be solved using graph projection splitting method[17,20] as described below.

$$\begin{aligned} &\underset{t\in\mathbb{R}^{mn},d\in\mathbb{R}^{l}}{\text{minimise}} \sum_{i\in\mathcal{I}_{VOIs}} h(d_i) + \sum_{j=1}^{m} \beta \|Lt[j]\|_1 \\ &\text{subject to} \quad \underset{t\geq 0,}{Dt = d}, \end{aligned} \tag{2}$$

where $D \in \mathbb{R}^{l\times mn}$ is a dose rate matrix, $t \geq 0$ is the element-wise non-negative emission time, d_i is the dose amount at the i-th voxel as introduced in Eq. (1). In Eq. (2),

$$h(d_i) \triangleq (\lambda_i^+ H(d_i - \hat{d}_i) + \lambda_i^- H(\hat{d}_i - d_i))(d_i - \hat{d}_i)^2,$$

where $H(x)$ is the unit step function with $H(a) = 1$ if $a > 0$, and $H(a) = 0$ if $a \leq 0$, and λ_i^+ and λ_i^- represent overdose and underdose penalty parameters for the i-th voxel, respectively. $\hat{d}_i$ represents the prescribed dose amount for the i-th voxel. $\hat{d}_i$ can have a different value for each VOI. For example, $\hat{d}_i = \hat{d}_{tumor}$ if $i \in \mathcal{I}_{tumor}$, and $\hat{d}_i = \hat{d}_{bladder}$ if $i \in \mathcal{I}_{bladder}$. The prescribed dose amount for HR-CTV, bladder, rectum, sigmoid, and normal tissue around the HR-CTV are denoted as $\hat{d}_{tumor}$, $\hat{d}_{bladder}$, $\hat{d}_{rectum}$, $\hat{d}_{sigmoid}$, and $\hat{d}_{normal}$, respectively. For λ_i^+ and λ_i^-, different non-negative overdose and underdose parameter values including 0 are used. For a vector $x \in \mathbb{R}^n$, $\|x\|_1$ is defined as the sum of the absolute value of each element of x, that is, $\|x\|_1 \triangleq \sum_{i=1}^{n} |x_i|$. The matrix $L \in \mathbb{R}^{n\times n}$ is introduced to calculate TV norm of a vector; namely, L is defined as follows:

$$L \triangleq \begin{bmatrix} 1 & -1 & 0 & 0 & \ldots & 0 & 0 \\ 0 & 1 & -1 & 0 & \ldots & 0 & 0 \\ 0 & 0 & 1 & -1 & \ldots & 0 & 0 \\ \vdots & \vdots & \vdots & \vdots & \vdots & \vdots & \vdots \\ 0 & 0 & 0 & 0 & \ldots & 1 & -1 \\ 0 & 0 & 0 & 0 & \ldots & 0 & 0 \end{bmatrix}.$$

The TV norm alleviates the positioning uncertainty in the treatment process. If two noticeably different emission times $t_{j,b}$ and $t_{j+1,b}$ between two adjacent beamlets along the same keyway are obtained, a small error in the dwell positions may cause an unacceptable treatment result. By applying the smoothness term between two adjacent beamlets along the same keyway in H-RSBT, the treatment error caused by the positioning uncertainty in the treatment process can be reduced.

Since different penalty parameter values for the overdose and underdose of a voxel are used, Eq. (2) is denoted as RSBT optimization problem having asymmetric penalty parameters or simply ADOS.

2.C.2. POGS implementation

In order to simplify the sum of the TV norms in Eq. (2), let us introduce a matrix $\bar{L} \triangleq I_{m\times m} \otimes L$, where $\otimes$ is the Kronecker product, and $I_{m\times m}$ is an $m\times m$ identity matrix. By assigning $\bar{L}t = y$ and introducing the indicator function $I(\cdot)$, Eq. (2) is restated as follows:

$$\begin{aligned} &\underset{t,y\in\mathbb{R}^{mn},d\in\mathbb{R}^{l}}{\text{minimise}} \sum_{i\in\mathcal{I}_{VOIs}} h(d_i) + \beta\|y\|_1 + I(t \geq 0) \\ &\text{subject to} \quad \underset{\bar{L}t = y}{Dt = d}, \end{aligned} \tag{3}$$

where $D \in \mathbb{R}^{l\times mn}$, $\bar{L} \in \mathbb{R}^{mn\times mn}$, and $I(t \geq 0)$ is the element-wise indicator function; namely, $I(t_i \geq 0) = 0$ if $t_i \geq 0$, and $I(t_i \geq 0) = \infty$ if $t_i < 0$.

By letting

$$A = \begin{pmatrix} D \\ \bar{L} \end{pmatrix}, \quad z = \begin{pmatrix} d \\ y \end{pmatrix},$$

Eq. (3) can be further simplified into

$$\begin{aligned} &\underset{t\in\mathbb{R}^{mn},z\in\mathbb{R}^{l+mn}}{\text{minimize}} \sum_{i=1}^{l} h(z_i) + \beta\|z_{[l+1:l+mn]}\|_1 + I(t\geq 0) \\ &\text{subject to} \quad At = z, \end{aligned} \tag{4}$$

where $z_{[a:b]}$ is the partial vector of z by taking vector z from the a-th element to the b-th element. The following functions are defined as

$$g(t) = I(t\geq 0), \tag{5}$$

$$f(z) = \sum_{i=1}^{l} h(z_i) + \beta\|z_{[l+1:l+mn]}\|_1. \tag{6}$$

Then Eq. (4) is converted into a graph-form convex optimization problem,[17] where the constraint is $z = At$, and $A = [D^T \bar{L}^T]^T \in \mathbb{R}^{(l+mn)\times mn}$. The detailed updating rules for each optimization variable in the POGS solver for Eq. (4) are described below. The derived results in detail for the proximal operators used in the POGS solver, updating steps, and stopping criteria are introduced as follows.

The POGS updates primal variables, conducts the projection onto the space $z = At$, and then, updates dual variables iteratively until the stopping criteria are satisfied or the maximum number of iterations, denoted by *MaxItr*, is reached. The primal variable and dual variable are updating variables to be used for optimality condition in the algorithm. For the primal variable, dual variable, and projection result, $(\hat{t},\hat{z})$, (t,z), and $(\tilde{t},\tilde{z})$ are used, respectively. Each updating step is introduced in detail for the optimization problem in Eq. (4). The super-script k is used to represent the k-th iteration.

Updating primal variables $\hat{t}^{k+1}$ and $\hat{z}^{k+1}$: In updating the primal variables, the following proximal operators with a penalty parameter ρ are used:

$$\begin{aligned} \hat{t}^{k+1} &= Prox_g(t^k - \tilde{t}^k) \\ &= \underset{t}{argmin} \;\; I(t\geq 0) + \frac{\rho}{2}\|t - (t^k - \tilde{t}^k)\|^2, \\ \hat{z}^{k+1} &= Prox_f(z^k - \tilde{z}^k) \\ &= \underset{z}{argmin} \;\; \sum_{i=1}^{l} h(z_i) + \beta\|z_{[l+1:l+mn]}\|_1 \\ &\qquad + \frac{\rho}{2}\|z - (z^k - \tilde{z}^k)\|^2. \end{aligned}$$

The proximal operator is used to make a compromise between the solution at the k-th iteration and the function value with the solution at the k+1 iteration. Closed-form formulas for the proximal operators can be explicitly derived. $\hat{t}^{k+1} \in \mathbb{R}^{mn}$ is stated as follows:

$$\hat{t}^{k+1} = max(t^k - \tilde{t}^k, \mathbf{0}), \tag{7}$$

where $max(a,b)$ provides the maximum value between a and b element-wise. $\hat{z}_i^{k+1}$, $1\leq i\leq l$ is derived as follows:

$$\hat{z}_i^{k+1} = \begin{cases} z_i^k - \tilde{z}_i^k - \frac{\beta}{\rho}, & \text{if } z_i^k - \tilde{z}_i^k > \frac{\beta}{\rho} \\ z_i^k - \tilde{z}_i^k + \frac{\beta}{\rho}, & \text{if } z_i^k - \tilde{z}_i^k < -\frac{\beta}{\rho} \\ 0, & \text{otherwise} \end{cases}. \tag{8}$$

For $\hat{z}_i^{k+1}$, l+1 ≤ i ≤ l+mn, the following derivation is obtained:

$$\hat{z}_i^{k+1} = \begin{cases} \frac{2\lambda_i^+\hat{d}_i + \rho(z_i^k - \tilde{z}_i^k)}{2\lambda_i^+ + \rho}, & \text{if } z_i^k - \tilde{z}_i^k \geq \hat{d}_i, \\ \frac{2\lambda_i^-\hat{d}_i + \rho(z_i^k - \tilde{z}_i^k)}{2\lambda_i^- + \rho}, & \text{if } z_i^k - \tilde{z}_i^k < \hat{d}_i. \end{cases} \tag{9}$$

POGS uses the adaptive value for ρ as default to further increase the convergence speed.

Projection onto $z = At$ from $(\hat{t}^{k+1} + \tilde{t}^k, \hat{z}^{k+1} + \tilde{z}^k)$: The projection operation is mapping the primal variables to the closest feasible solution. The projected variables onto $z = At$ from $(\hat{t}^{k+1} + \tilde{t}^k, \hat{z}^{k+1} + \tilde{z}^k)$, denoted as t^{k+1} and z^{k+1}, are obtained by solving the following optimization:

$$\begin{aligned} &\underset{t,z}{\text{minimize}} \quad \frac{1}{2}\|t - (\hat{t}^{k+1} + \tilde{t}^k)\|_2^2 + \frac{1}{2}\|z - (\hat{z}^{k+1} + \tilde{z}^k)\|_2^2 \\ &\text{subject to} \quad At = z \end{aligned}$$

By solving this optimization and using Lagrange conditions,[21] the following formulation is obtained:

$$\begin{pmatrix} t^{k+1} \\ z^{k+1} \end{pmatrix} = \begin{pmatrix} I & A^T \\ A & -I \end{pmatrix}^{-1} \begin{pmatrix} \hat{t}^{k+1} + \tilde{t}^k + A^T(\hat{z}^{k+1} + \tilde{z}^t) \\ 0 \end{pmatrix}.$$

Updating dual variables $\tilde{t}^{k+1}$ and $\tilde{z}^{k+1}$: The dual variable at iteration (k+1) is obtained by updating the dual variable at the k-th iteration as follows:

$$\begin{aligned} \tilde{t}^{k+1} &= \tilde{t}^k + \hat{t}^{k+1} - t^{k+1}, \\ \tilde{z}^{k+1} &= \tilde{z}^k + \hat{z}^{k+1} - z^{k+1}. \end{aligned}$$

Algorithm 1 summarises the updating steps.

Stopping criteria: For the stopping criteria, the primal and dual residuals are defined as follows:

$$\begin{aligned} &\|A\hat{t}^{k+1} - \hat{z}^{k+1}\|_2 \leq \epsilon^{pri}, \\ &\|A^T\hat{v}^{k+1} + \hat{\mu}^{k+1}\|_2 \leq \epsilon^{dual}, \end{aligned} \tag{10}$$

where $\hat{v}^{k+1} = -\rho(\hat{z}^{k+1} - z^k + \tilde{z}^k)$, $\hat{\mu}^{k+1} = -\rho(\hat{t}^{k+1} - t^k + \tilde{t}^k)$. Here, ϵ^{pri} and $\epsilon^{dual}$are positive tolerances for primal and dual residuals, respectively:

$$\begin{aligned} \epsilon^{pri} &= \epsilon^{abs} + \epsilon^{rel}\|\hat{z}^{k+1}\|_2, \\ \epsilon^{dual} &= \epsilon^{abs} + \epsilon^{rel}\|\hat{\mu}^{k+1}\|_2, \end{aligned} \tag{11}$$

where (ϵ^{abs}, ϵ^{abs})=(10^{-4},10^{-2}) were used in the numerical experiments.

Algorithm 1: Fast treatment planning for RSBT in POGS implementation

Input: $A \in \mathbb{R}^{(l+mn)\times mn}$, *MaxItr*, $\lambda^+, \lambda^-, \hat{d} \in \mathbb{R}^l$, β

Output: t

Initialize: $k\leftarrow 0$, $t^k\leftarrow 0$, $z^k\leftarrow 0$, $\tilde{t} \leftarrow 0$, $\tilde{z} \leftarrow 0$

for k = 1 **to** MaxItr **do**

Updating primal variables $\hat{t}^{k+1}$, $\hat{z}^{k+1}$:

Algorithm 1. Continued.

Algorithm 1: Fast treatment planning for RSBT in POGS implementation

$\hat{t}^{k+1} \leftarrow Prox_g(t^k - \tilde{t}^k)$ ▷ See (7)

$\hat{z}^{k+1} \leftarrow Prox_f(z^k - \tilde{z}^k)$ ▷ See (8) and (9)

Projection onto $z = At$:

$$\begin{pmatrix} t^{k+1} \\ z^{k+1} \end{pmatrix} \leftarrow \begin{pmatrix} I & A^T \\ A & -I \end{pmatrix}^{-1} \begin{pmatrix} \hat{t}^{k+1} + \tilde{t}^k + A^T(\hat{z}^{k+1} + \tilde{z}^t) \\ 0 \end{pmatrix}$$

Updating dual variables $\tilde{t}^{k+1}$, $\tilde{z}^{k+1}$:

$\tilde{t}^{k+1} \leftarrow \tilde{t}^k + \hat{t}^{k+1} - t^{k+1}$

$\tilde{z}^{k+1} \leftarrow \tilde{z}^k + \hat{z}^{k+1} - z^{k+1}$

if *Stopping criteria are met* **then**

break

end

end

2.D. Treatment planning

This study used the same dataset as the previous studies by Liu et al.[15] and Dadkhah et al.,[5] which included five patients treated for cervical cancer with HR-CTV volumes ranging from 42.2 to 98.8 cm^3. Table I shows the volume and maximum dimension of HR-CTV for five patients. All the HR-CTVs and OARs were manually contoured by physicians on T2 weighted $1 \times 1 \times 3$ mm^3 resolution MR images taken with a Siemens MAGNETOM 3T scanner (Siemens, Germany) at the beginning of the first fraction of brachytherapy. A titanium Fletcher–Suit–Delclos style tandem and ovoids (Varian Medical Systems, Palo Alto, CA, USA) were used as the brachytherapy applicator.

All the patients had external beam radiation treatment in 25 fractions at 1.8 Gy/fraction. It was assumed that the external beam radiotherapy dose was delivered equally to all of the voxels in HR-CTV for all the patient cases. The dose in each voxel was converted to equivalent dose in 2 Gy per fraction of external radiation therapy (EQD2) using the linear quadratic model,[22] where the linear-quadratic parameter, α/β, is set to 3 Gy for OARs and 10 Gy for HR-CTV.

For VOIs, the voxels located at a distance between 3 mm and 20 mm to the radiation source path or those within 10 mm inside and outside of the HR-CTV boundary surface were included.[15] The HR-CTV, HR-CTV boundary, bladder, sigmoid, and rectum inside of VOIs in the optimization problem were considered. The optimization parameter settings are shown in Table II. Table III shows the dimension of the dose matrix D in Eqn. (2).

For all the brachytherapy treatment plans, the EQD2 of the HR-CTV was escalated without exceeding the D_{2cc} tolerance of the bladder, rectum, and sigmoid colon. 90 Gy for bladder tolerance, and 75 Gy for rectum and sigmoid colon tolerances were used according to Groupe Européen de Curiethérapie, European Society for Therapeutic Radiology and Oncology (GEC ESTRO).[23,24]

Since the goal of this research is to achieve a fast solution to the RSBT dose optimization problem without compromising the plan quality, the execution times to solve Eq. (2) were compared for all five patient cases. The numerical experiments were conducted on HP Z220 CMT with an Intel Core i7-3770 dual core CPU @3.4 GHz clock speed and 16 GB DDR3 RAM, using Matlab (R2013b) on the Windows 7 operating system.

TABLE I. HR-CTV volumes and dimensions for all patients.

Patient num.	HR-CTV volume (cm^3)	HR-CTV maximum dimension (cm)
Case 1	42.2	6.3
Case 2	45.8	7.4
Case 3	78.0	8.6
Case 4	98.8	9.6
Case 5	75.0	7.5
Avg.	68.0	7.9
SD[a]	23.8	1.8

[a]Standard deviation.

2.E. Treatment plan evaluation

Optimized treatment plans were generated for all patients using the POGS method and the previously investigated CPLEX method.[15] The same objective function, with the same input parameters and beamlets, was minimized for each patient with both methods. A total variation term was included in the objective function as a regularization term, resulting in smoothly varying emission times along each keyway. The regularization promotes robustness of the resulting overall dose distribution with respect to small errors (expected $\leq$ 1 mm) in source positioning. The rectum, bladder, sigmoid colon, HR-CTV, and HR-CTV boundary were the structures considered.

POGS method was compared with the previous research conducted by Liu et al.[15] using CPLEX[16] for H-RSBT. It was evaluated that the quality of the delivery plans as well as the execution time to solve Eq. (2) with POGS.[17]

The comparison metrics for the quality of the delivery plans are the HR-CTV D_{90}, HR-CTV D_{100}, D_{2cc} of all OARs, DVH, and dose distributions considered.

3. RESULTS

Results for five cervical cancer patient cases are shown in Table IV. Figure 2 shows the corresponding DVH in H-RSBT. With the same parameter settings as in Table II, POGS can achieve an RSBT plan with almost the same D_{90} value (less than 1% difference) as that achieved by CPLEX in each of the five patient cases. D_{2cc} values for OARs obtained by POGS are within 1% of the values obtained using CPLEX. For the execution time, approximately 18 times faster speed to solve the ADOS problem for H-RSBT was achieved than the CPLEX-based method on average. For all patients, total optimization times were 32.1–65.4 s for CPLEX and 2.1–3.9 s for POGS.

TABLE II. Parameter settings.

Method	$\hat{d}_{tumor}$	$\hat{d}_{bladder}$	$\hat{d}_{rectum}$	$\hat{d}_{sigmoid}$	$\hat{d}_{normal}$[a]	Tumor λ_i^+/λ_i^-	Bladder λ_i^+/λ_i^-	Rectum λ_i^+/λ_i^-	Sigmoid λ_i^+/λ_i^-	Normal[b] λ_i^+/λ_i^-	β
CPLEX	40	25	20	20	40	0/ 2	2/0	2/0	2/0	2/0	100
POGS	40	25	20	20	40	0/ 2	2/0	2/0	2/0	2/0	100

[a]Prescribed dose for tumor boundary.
[b]Penalty parameter for tumor boundary.

TABLE III. Dimension of $D \in \mathbb{R}^{l\times mn}$ in Eq. (2).

Patient num.	$l\times mn$
Case 1	54693 × 144
Case 2	51109 × 126
Case 3	79065 × 222
Case 4	50680 × 144
Case 5	59220 × 228

Figure 3 shows that the EQD2 dose distributions were nearly identical for both methods.

4. DISCUSSION

Studying optimization algorithms in radiotherapy aims to reduce the treatment planning time as well as to improve the quality of the treatment. Especially, the inverse planning by simulated annealing (IPSA) technique optimizes the DVH directly with given constraints in heuristic way[6] and is used in clinical treatment planning system of Oncentura (Elekta Inc., Atlanta, GA, USA).[11] The IPSA has been reported as favorable dosimetric plans.[25] However, due to its heuristic nature, resulting increased degree of freedom, and its nonconvex optimization problem, the IPSA suffers from its computational time[26] and a global solution is not guaranteed. Thus, its solution may not be clinically robust enough. Instead of directly optimizing DVH, the ADOS optimization problem is expressed as a convex optimization problem. Both CPLEX and POGS provide the same globally optimal solutions, but POGS presented 18 times fast computational efficacy.

The proposed POGS method is not limited to RSBT. In general it is applicable to all intensity-modulated brachytherapy (IMBT) approaches including dynamic-modulated brachytherapy (DMBT),[27–31] conventional HDR-BT, and pulse-dose-rate (PDR) brachytherapy for which the previously tested optimization techniques such as dose-surface optimization (DSO) and IPSA are implemented. In this study, the proposed POGS was only compared with CPLEX optimization technique, since the previous study[15] had compared the CPLEX optimization method with other clinically available approaches such as DSO and IPSA. The CPLEX algorithm was found as efficient in optimization time and effective in plan quality for RSBT techniques when compared to other clinically available approaches of DSO and IPSA.

The POGS algorithm can be thought of as the engine that enables shield angle selection algorithms, which require multiple optimizations having different azimuthal angles to be run quickly, to operate quickly enough for clinical implementation. For example, with all 72 possible beam angles of multiples of 5 degrees for possible shield angle selection, POGS takes about 3.2 min (2.7 s × 72 = 194.4 s), while CPLEX takes about 57.5 min (47.9 s × 72 = 3448.8 s), where 2.7 s and 47.9 s are the average execution time to solve the optimization problem in Table IV. In this case, the operation time to solve the RSBT optimization problem becomes a burden to

TABLE IV. Comparison between POGS and CPLEX for 45° azimuthal angle.

Case	Method	HR-CTV D_{90} (Gy)	HR-CTV D_{100} (Gy)	Bladder D_{2cc} (Gy)	Rectum D_{2cc} (Gy)	Sigmoid D_{2cc} (Gy)	Execution Time (s)
Case 1	CPLEX	110.8	54.0	89.9	62.4	75.0	32.1
	POGS	111.4	54.0	90.0	64.7	74.7	2.1
Case 2	CPLEX	111.5	44.3	90.0	72.2	54.4	37.0
	POGS	111.5	44.3	90.0	71.7	54.8	2.1
Case 3	CPLEX	96.0	44.3	85.9	57.3	75.0	65.4
	POGS	95.0	44.3	85.2	55.1	75.0	3.9
Case 4	CPLEX	107.0	55.3	90.0	69.9	54.0	39.4
	POGS	106.9	55.4	90.0	69.8	54.0	2.3
Case 5	CPLEX	112.7	44.3	90.0	68.1	59.2	65.4
	POGS	112.7	44.3	90.0	68.1	59.2	3.2
Average	CPLEX	107.6	48.4	89.2	66.0	63.5	47.9
	POGS	107.5	48.5	89.0	65.9	63.5	2.7

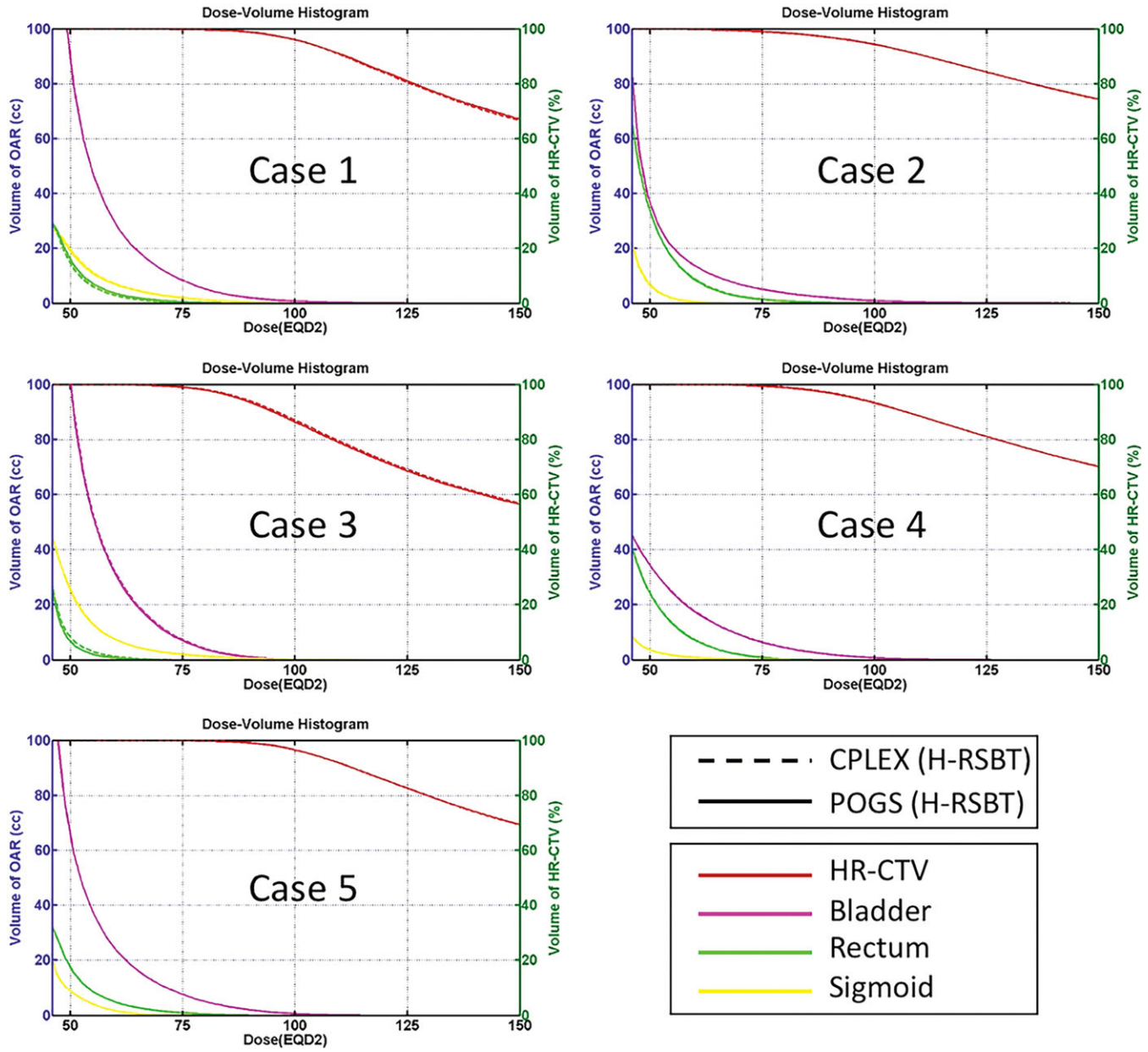

FIG. 2. Dose volume histograms (DVH) of all treatment planning for five patient cases in H-RSBT with 45° azimuthal angle. [Color figure can be viewed at wileyonlinelibrary.com]

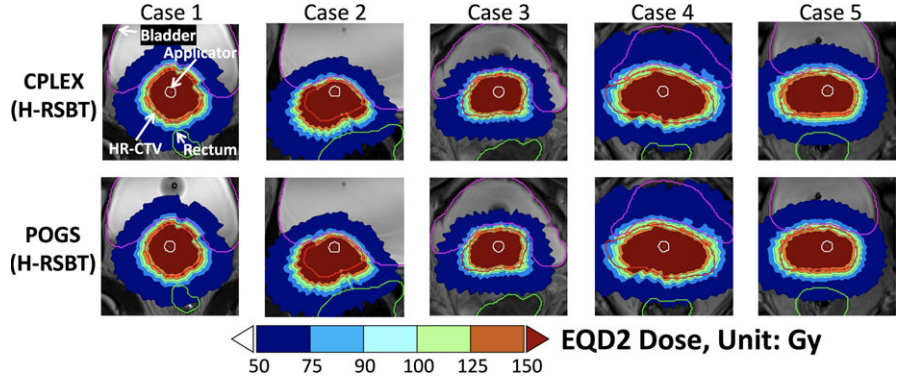

FIG. 3. EQD2 dose distributions on MR images for five patient cases obtained from CPLEX and POGS with H-RSBT using 45° azimuthal angle. [Color figure can be viewed at wileyonlinelibrary.com]

use in clinic, and the clinical benefit of using the POGS algorithm can be much clearly shown.

A partial shield with 45° azimuthal angle in H-RSBT was used for the numerical experiments. However, finding the optimal shield angle in H-RSBT is still under investigation. It may be possible to find the optimal shield angle (opening) and the radiation exposure time for each beamlet by including different dose matrices obtained with different angle sizes in the optimization problem.

For the purpose of comparison study, VOIs were applied to reduce the size of the ADOS optimization problem. Instead of applying VOIs, all voxels can be included in the optimization problem under the expectation of better treatment quality with heavy computation. Since parallel computing and GPU-based high performance computing can play an important role in solving extremely large-scale optimization problems, there is a rising question about the usability of POGS in parallel computing environment or GPU-based implantation. The implementation of POGS in such environment is beyond the scope of this study.

POGS (and ADMM) has been used in previous research on intensity-modulated radiation therapy (IMRT),[17,32] fluence map optimization,[33] and external beam radiotherapy (EBRT) optimization.[34] To the best of our knowledge, our paper is the first work to use POGS in brachytherapy, including the mechanically feasible delivery system called H-RSBT.

While H-RSBT uses a shield around catheter of radiation source which is inserted into a brachytherapy applicator with helical keyways, DMBT approach is performed using a direction-modulated brachytherapy tandem with peripheral holes, called core, in which high-dose radiation source is placed and translated longitudinally, and the core in DMBT provides a substantial amount of shielding around the source.[31] However, due to the presence of a fairly thick tungsten core in DMBT applicator, this technique is not an MRI compatible technique while both conventional HDR-BT, which is performed in the absence of any shielding material around the source, and H-RSBT techniques are MR-compatible. Due to the similar mechanisms among HDR-BT, H-RSBT, and DMBT, the proposed POGS method is also applicable to HDR-BT as well as DMBT with modifications on dose matrix and TV norm.

5. CONCLUSIONS

POGS substantially reduced treatment plan optimization time around 18 times for RSBT with similar HR-CTV D_{90}, OAR D_{2cc} values, and EQD2 dose distributions compared to those obtained using CPLEX, which is significant progress toward clinical implementation of RSBT. For all cervical cancer patients, total optimization times were 32.1–65.4 s for CPLEX and 2.1–3.9 s for POGS.

ACKNOWLEDGMENTS

The authors thank the generous support from NIH 1R01EB020665 and NSF DMS-1418737. The authors also thank Jianfeng Cai, Qihang Lin, and Haiye Huo for discussions and advice on paper writing.

[a]Author to whom correspondence should be addressed. Electronic mail: xiaodong-wu@uiowa.edu.

REFERENCES

1. Pötter R, Dimopoulos J, Georg P, et al. Clinical impact of MRI assisted dose volume adaptation and dose escalation in brachytherapy of locally advanced cervix cancer. *Radiother Oncol*. 2007;83:148–155.
2. Kirisits C, Lang S, Dimopoulos J, Berger D, Georg D, Po¨tter R. The vienna applicator for combined intracavitary and interstitial brachytherapy of cervical cancer: design, application, treatment planning, dosimetric results. *Int J Radiat Oncol Biol Phys*. 2006;65:624–630.
3. Ebert MA. Possibilities for intensity-modulated brachytherapy: technical limitations on the use of non-isotropic sources. *Physics in medicine and biology*. 2002;47:2495.
4. Ebert M. Potential dose-conformity advantages with multi-source intensity-modulated brachytherapy (IMBT). *Australas Phys Eng Sci Med*. 2006;29:165–171.
5. Dadkhah H, Kim Y, Wu X, Flynn RT. Multihelix rotating shield brachytherapy for cervical cancer. *Med Phys*. 2015;42:6579–6588.
6. Lessard E, Pouliot J. Inverse planning anatomy-based dose optimization for HDR-brachytherapy of the prostate using fast simulated annealing algorithm and dedicated objective function. *Med Phys*. 2001;28:773–779.
7. Akimoto T, Katoh H, Kitamoto Y, Shirai K, Shioya M, Nakano T. Anatomy-based inverse optimization in high-dose-rate brachytherapy combined with hypofractionated external beam radiotherapy for localized prostate cancer: comparison of incidence of acute genitourinary toxicity between anatomy-based inverse optimization and geometric optimization. *Int J Radiat Oncol Biol Phys*. 2006;64:1360–1366.
8. Baltas D, Katsilieri Z, Kefala V, et al. Influence of modulation restriction in inverse optimization with HIPO of prostate implants on plan quality: analysis using dosimetric and radiobiological indices. In: Dössel O, Schlegel WC, eds. *Proceedings of World Congress on Medical Physics and Biomedical Engineering*. Berlin: Springer Berlin; 2009:283–286.
9. Citrin D, Ning H, Guion P, et al. Inverse treatment planning based on MRI for HDR prostate brachytherapy. *Int J Radiat Oncol Biol Phys*. 2005;61:1267–1275.
10. DeWitt KD, Hsu ICJ, Speight J, Weinberg VK, Lessard E, Pouliot J. 3D inverse treatment planning for the tandem and ovoid applicator in cervical cancer. *Int J Radiat Oncol Biol Phys*. 2005;63:1270–1274.
11. Manikandan A, Sarkar B, Rajendran VT, et al. Role of step size and max dwell time in anatomy based inverse optimization for prostate implants. *J Med Phys*. 2013;38:148.
12. Jacob D, Raben A, Sarkar A, Grimm J, Simpson L. Anatomy-based inverse planning simulated annealing optimization in high-dose-rate prostate brachytherapy: significant dosimetric advantage over other optimization techniques. *Int J Radiat Oncol Biol Phy.* 2008;72:820–827.
13. Liu Y, Flynn RT, Yang W, et al. Rapid emission angle selection for rotating-shield brachytherapy. *Med Phys*. 2013;40:051720.
14. Yang W, Kim Y, Wu X, et al. Rotating-shield brachytherapy for cervical cancer. *Phys Med Biol*. 2013;58:3931.
15. Liu Y, Flynn RT, Kim Y, Wu X. Asymmetric dose-volume optimization with smoothness control for rotating-shield brachytherapy. *Med Phys*. 2014;41:111709.
16. IBM. IBM ILOG CPLEX, optimizer, https://www-01.ibm.com/software/commerce/optimization/cplex-optimizer/; 2017.
17. Fougner C, Boyd S. Parameter selection and pre-conditioning for a graph form solver. In: Tempo R, Yurkovich S, Misra P, eds. *Emerging Applications of Control and System Theory*. 2017.
18. Rivard MJ, Davis SD, DeWerd LA, Rusch TW, Axelrod S. Calculated and measured brachytherapy dosimetry parameters in water for the Xoft Axxent X-Ray source: an electronic brachytherapy source. *Med Phys*. 2006;33:4020–4032.

19. Velpula KK, Rehman AA, Chigurupati S, Sanam R, Inampudi KK, Akila CS. Computational analysis of human and mouse CREB3L4 protein. *Bioinformation*. 2012;8:574.
20. Parikh N, Boyd S. Block splitting for distributed optimization. *Math Program Comput*. 2014;6:77–102.
21. Boyd S, Vandenberghe L. *Convex optimization*. New York: Cambridge University Press; 2004.
22. Joiner MC, Van der Kogel A. *Basic clinical radiobiology.* Abingdon, Oxon: CRC Press; 2016.
23. Po¨tter R, Haie-Meder C, Limbergen EV, et al. Recommendations from gynaecological (GYN) GEC-ESTRO working group (II): Concepts and terms in 3D image-based treatment planning in cervix cancer brachytherapy-3D dose volume parameters and aspects of 3D image-based anatomy, radiation physics, radiobiology. *Radiother Oncol*. 2006;78:67–77.
24. Haie-Meder C, Po¨tter R, Van Limbergen E, et al. Recommendations from gynaecological (GYN) GEC-ESTRO working group (I): concepts and terms in 3D image based 3D treatment planning in cervix cancer brachytherapy with emphasis on MRI assessment of GTV and CTV. *Radiother Oncol*. 2005;74:235–245.
25. Morton GC, Sankreacha R, Halina P, Loblaw A. A comparison of anatomy-based inverse planning with simulated annealing and graphical optimization for high-dose-rate prostate brachytherapy. *Brachytherapy.* 2008;7:12–16.
26. Shi C, Guo B, Cheng C-Y, Esquivel C, Eng T, Papanikolaou N. Three dimensional intensity modulated brachytherapy (IMBT): dosimetry algorithm and inverse treatment planning. *Med Phys*. 2010;37:3725–3737.
27. Han DY, Scanderbeg DJ, Yashar C, Song WY. The use of DMBT-concept T&O applicator in cervical cancer: a case study. *Brachytherapy.* 2017;14:S64–S65.
28. Han DY, Webster MJ, Scanderbeg DJ, et al. Direction-modulated brachytherapy for high-dose-rate treatment of cervical cancer. I: Theoretical design. *Int J Radiat Oncol Biol Phys*. 2014;89:666–673.
29. Webster MJ, Devic S, Vuong T, et al. HDR brachytherapy of rectal cancer using a novel grooved-shielding applicator design. *Med Phys*. 2013;40:091704.
30. Webster MJ, Devic S, Vuong T, et al. Dynamic modulated brachytherapy (DMBT) for rectal cancer. *Med Phys*. 2013;40:011718.
31. Webster MJ, Scanderbeg DJ, Watkins WT, Stenstrom J, Lawson JD, Song WY. Dynamic modulated brachytherapy (DMBT): concept, design, system development. *Brachytherapy.* 2011;10:S33–S34.
32. Zarepisheh M, Xing L, Ye Y. A computation study on an integrated alternating direction method of multipliers for large scale optimization. *Optim Lett*. 2017;1–13.
33. Gao H. Robust fluence map optimization via alternating direction method of multipliers with empirical parameter optimization. *Phys Med Biol*. 2016;61:2838.
34. Liu X, Pelizzari C, Belcher AH, Grelewicz Z, Wiersma RD. Use of proximal operator graph solver for radiation therapy inverse treatment planning. *Med Phys*. 2017;44:1246–1256.